bioRxiv preprint doi: https://doi.org/10.1101/2024.04.10.588509; this version posted April 14, 2024. The copyright holder for this preprint (which was not certified by peer review) is the author/funder, who has granted bioRxiv a license to display the preprint in perpetuity. It is made available under aCC-BY-NC-ND 4.0 International license.

Neurovascular coupling and briefCO_2 interrogate distinct vascular regulations

Marine Tournissac*[1,2], Emmanuelle Chaigneau[1], Sonia Pfister[3], Ali-Kemal Aydin[1], Yannick Goulam Houssen[1], Philip O'Herron[4], Jessica Filosa[4], Mayeul Collot[3], Anne Joutel[2], Serge Charpak*[1]

[1] Sorbonne Université, Inserm U968, Vision Institute, Paris, France
[2] Université Paris Cité, Institute of Psychiatry and Neuroscience of Paris (IPNP), INSERM U1266, 75014 Paris, France
[3] Chemistry of Photoresponsive Systems, Laboratoire de Chémo-Biologie Synthétique et Thérapeutique (CBST) UMR 7199, CNRS, Université de Strasbourg, F-67400 Illkirch, France
[4] Department of Physiology, Augusta University, Augusta, GA, USA

These authors contributed equally to this work: Emmanuelle Chaigneau, Sonia Pfister.

*E-mail: marine.tournissac@inserm.fr; serge.charpak@inserm.fr

Abstract

Neurovascular coupling (NVC), which mediates rapid increases in cerebral blood flow in response to neuronal activation, is commonly used to map brain activation or dysfunction. Here we tested the reemerging hypothesis that CO_2 generated by neuronal metabolism contributes to NVC. We combined functional ultrasound and two-photon imaging in the mouse barrel cortex to examine specifically the onsets of local changes in vessel diameter, blood flow dynamics, vascular/perivascular/intracellular pH, and intracellular calcium signals along the vascular arbor in response to briefCO_2, a short and strong hypercapnic challenge (10 s, 20%) and whisker stimulation. We report that briefCO_2 reversibly acidifies all cells of the arteriole wall and the periarteriolar space 3-4 seconds prior to the arteriole dilation. During this prolonged lag period, NVC triggered by whisker stimulation is not affected by the acidification of the entire neurovascular unit. As it also persists under condition of continuous inflow of CO_2, we conclude that CO_2 is not involved in NVC.

Introduction

Human brain functional imaging uses functional hyperemia, a rapid and local increase in blood flow, to map brain regions activated by sensory stimulation and behavioral tasks, as well as assess brain connectivity. The signaling pathways by which neurovascular coupling (NVC) generates functional hyperemia involve the cooperation of numerous cell types, and it has long been accepted that these pathways are triggered by neurotransmitter feedforward mechanisms rather than from local metabolic feedback due to acute oxygen and glucose consumption, or CO_2 production[1,2]. Several arguments were successively raised and put aside in support of the metabolic feedback hypothesis. Initial measurements of partial pressure of oxygen (pO_2) with Clark electrodes, performed in the brain parenchyma of anesthetized animals with acute craniotomies[3–5], reported that sensory stimulation generated local pO_2 dips, the timing of which was compatible with a triggering role in NVC[6]. This hypothesis was however recently questioned, as the pO_2 dip disappeared in chronically-prepared awake mice, i.e., more akin to physiological conditions[7]. The triggering role of oxygen in NVC is therefore unlikely, even though one study reported that local application of O_2 scavengers could generate a pO_2 dip and an increase in blood flow[8]. Concerning glucose, acute hyperglycemia was recently shown to result in decreased NVC in the zebrafish optic tectum[9], whereas other experiments have reported that NVC is unaffected by hypoglycemia[10,11]. The role of CO_2 production as a trigger of NVC was initially discarded because synaptic activation *in vivo* generates an alkalinization of the

bioRxiv preprint doi: https://doi.org/10.1101/2024.04.10.588509; this version posted April 14, 2024. The copyright holder for this preprint (which was not certified by peer review) is the author/funder, who has granted bioRxiv a license to display the preprint in perpetuity. It is made available under aCC-BY-NC-ND 4.0 International license.

extracellular fluid[12–14], which should constrict, rather than dilate, smooth muscle cells (SMCs)[15]. On the other hand, in the mouse cortex, the extracellular alkalinization can be reversed to a rapid acidosis upon blockade of the sodium bicarbonate co-transporter 1 (NBCe1) in astrocytes[13], suggesting that the dynamics of CO_2 production, normally buffered by astrocytes, is fast enough to participate in NVC. Because some studies also suggested that CO_2 *per se*, independent of pH, has a direct effect on SMCs relaxation during cerebrovascular reactivity to CO_2 (CVR_{CO2}), and that CO_2, in addition to passive diffusion through cell membranes can diffuse through selective gas channels (for review see[16]), the role of CO_2 production in NVC has reemerged. In particular, Hosford *et al.* recently used an "occlusion or saturation" protocol to investigate the issue in rodents[17], in which, upon breathing CO_2 (10%) over a 10-minute period, vascular responses to electrical stimulation of the paw were abolished, even when resting blood flow was maintained at a constant rate with indomethacin and caffeine. They proposed that exogenous CO_2 diffusing from the bloodstream was saturating CO_2 dependent processes, *i.e.,* masking the effect of CO_2 produced by neuronal metabolism. Endogenous CO_2 would thus mediate a feedback mechanism involving NBCe1, leading to CO_2 removal through functional hyperemia. As both NVC and CVR_{CO2} are widely used in clinics, this controversial hypothesis requires further support and characterization of the possible sites of action of CO_2 produced by neurons along the vascular arbor. Here, we synthetized a novel vascular pH sensor and used the barrel cortex neurovascular model, in chronic sedated mice, to investigate the interactions between NVC and CO_2. We first characterized a new CO_2 stimulus, brief and strong (subsequently referred to as "briefCO_2"), that triggers vascular responses within only a couple of seconds. We then precisely measured the onsets of GCaMP6/8 fluorescence changes in cells of the neurovascular unit, and pH and blood flow responses along the vascular arbor following briefCO_2. The analysis of CVR to briefCO_2 and NVC response onsets and interactions, at both the microscopic and mesoscopic level, indicate that CO_2 does not play a role in NVC.

Results

briefCO_2 stimulation causes early and delayed responses

To investigate the potential role of CO_2 in NVC, we applied a systematic approach based on timing measurements of physiological responses, which enabled us to uncover compartmentalization of vascular responses during NVC[18]. In contrast to many previous works that studied CVR_{CO2} using long lasting CO_2 stimulations, on the order of several minutes, to reach a steady state (for reviews on CVR_{CO2} see[19–21]), we tested the effect of briefCO_2, a 10 s inhalation of 20% CO_2 to generate sharp, reversible and reproducible vascular and cellular responses. All experiments were done after a 7-10 day recovery period from surgery and under sedation with dexmedetomidine, as we found that briefCO_2, even at 5% CO_2, is too stressful to train awake mice. Under sedation, responses to briefCO_2 could be reproduced up to 20 times per experiment (at 5 minutes inter-trial intervals), and over months without any observable adverse effects.

Fig. 1 illustrates that briefCO_2 triggered an early increase of breathing frequency about 2 seconds after the beginning of CO_2 application (mean onset of 1.8 ± 1 s, n = 19 animals, 30 experiments), whereas it required about 3-4 additional seconds to dilate both pial and penetrating arterioles (mean onset for all arterioles, 5.8 ± 1.4 s, n = 23 animals, 29 experiments; see also Supplementary Movie 3). Note that pial arteriole diameter was directly measured using two-photon microscopy line-scan acquisitions, whereas for penetrating arterioles the diameter was calculated from the lumen area measured with movie acquisitions (see Methods). As baseline diameter fluctuates at 0.1 Hz due to vasomotion[22,23], vessel diameter changes were expressed in z score to improve the precision of dilation onsets, and to minimize the contribution of trials and vessels with the largest 0.1 Hz diameter fluctuations (see our previous work[24] and Methods). Dilation onsets were determined using an approach based on fits (onset is defined as the time to reach 10% of the peak of the fit; see Methods).

bioRxiv preprint doi: https://doi.org/10.1101/2024.04.10.588509; this version posted April 14, 2024. The copyright holder for this preprint (which was not certified by peer review) is the author/funder, who has granted bioRxiv a license to display the preprint in perpetuity. It is made available under aCC-BY-NC-ND 4.0 International license.

As dilation can be associated with an increase or decrease in blood velocity[18], we performed simultaneous measurements of the pial arteriole diameter and blood velocity with broken line-scans (Fig. 2a). Fig. 2b illustrates that surprisingly, briefCO_2 was followed by an early decrease in velocity (average onset of 2.9 ± 0.6 s, n = 7 vessels, 6 mice). As a result, blood flow (calculated as πR^2* velocity) increased over resting flow with a large delay of 7.5 s ± 2.4 s (time to reach 10% over the baseline; n = 7 vessels, 6 mice). Dilation and velocity changes amounted to about 10% (Fig. 2b inset; see also Supplementary Fig. 1). Note that in 4 additional penetrating arterioles that had a small segment parallel to the image plane (i.e., in which velocity could be measured), briefCO_2 was also followed by an early decrease in blood velocity (average onset of 3.4 ± 0.9 s; n = 4 vessels, 3 mice), demonstrating that pial and penetrating arterioles respond similarly to briefCO_2. The uncoupling between blood flow and velocity responses was markedly different from what occurs during neurovascular coupling, where sensory stimulation triggers "simultaneous" increases of both velocity and vessel diameter in pial arterioles (see[24]). Thus, depending on the type of vascular signal reaching the pial arteriole, backpropagating during NVC or propagating downstream during briefCO_2, the regulation of blood functional parameters strongly differs.

The decrease in velocity during the 3-4 s period where the arteriole diameter remains constant implies that it results from an upstream event, e.g., occurring at the level of the middle cerebral artery, the circle of Willis, or the internal carotid. To support this hypothesis, we imaged the dynamics of cerebral blood volume (CBV) in depth using functional ultrasound imaging (fUS), an approach now well established in anesthetized and awake mice[25–27]. Fig. 2c-e shows that briefCO_2 resulted in an early drop of 10% of CBV in the internal carotid (mean onset of 2.0 ± 1.3 s; n = 6 experiments, 5 mice), which preceded the CBV increase in the cortex by 3 s (mean onset of 4.7 ± 1.5 s; n = 5 experiments, 5 mice, time to reach 10% over the baseline). Alignment of fUS CBV responses in the carotid and velocity responses in pial arterioles indicate that the CBV signal in the carotid underlies the early velocity drop (with constant diameter) in cortical arterioles (Fig. 2e inset). The carotid signal itself resulted from a transient and modest (~ 1 mmHg) drop of arterial pressure, which occurred rapidly during briefCO_2 (Supplementary Fig. 2c). To conclude, briefCO_2 resulted in early (velocity) and delayed (diameter) arteriole responses, with the early response being compatible with the time required for blood, acidified and transporting CO_2, to reach the carotid and brain arterioles[28].

pH/CO_2 underlies early GCaMP6/8 fluorescence changes in cells composing the arteriole NVU

To investigate which cell type contributed to the arteriolar dilation induced by briefCO_2, we measured the dynamics of GCaMP6 and GCaMP8 fluorescence in each cells of the arteriole neurovascular unit (NVU), i.e., in endothelial cells, SMCs, astrocyte end-feet and perivascular neurons in different strains of transgenic animals (Fig. 3a). Surprisingly, briefCO_2 decreased fluorescence in all cells of the NVU. In transgenic mice expressing GCaMP6 in SMCs, briefCO_2 resulted in a decrease in fluorescence 2-3 s before dilation (Fig. 3b, onset from CO_2 application: 3.3 ± 0.7 s; n = 6 vessels, 5 mice), contrasting to the rapid decrease that occurs during neurovascular coupling (Fig. 3a inset; see also[18]). In astrocytes and endothelial cells, this decrease in onset was variable but preceded arteriole dilation (endothelial cells: 3.3 ± 1.5 s, n = 8 vessels, 4 mice; astrocytes: 2.1 ± 0.6 s, n = 5 vessels, 4 mice). The dendritic neuropil onset (3.9 ± 1.3 s; n = 7 vessels, 5 mice) was not significantly different from the dilation onset. As GCaMP6/8 fluorescence is known to decrease with acidosis[29,30] and since fluorescence decreased in all NVU cells, we raised the hypothesis that briefCO_2 caused a decrease of intracellular pH rather than of intracellular calcium. We synthetized and injected intravenously a novel form of the fluorescent pH sensor H-Ruby[31] attached to a dextran (70 kDa) (Fig. 3c). The H-Ruby dextran conjugate displayed a 53-fold fluorescence enhancement at 580 nm (from pH 10 to 4.5) with a measured pKa of 7.57 ± 0.06. It did not leak from blood and, when co-injected intravenously with AlexaFluor488 (AF488, not sensitive to pH) also attached to a 70 kDa dextran, allowed for the quantification of vascular pH changes from fluorescence ratio measurements (see Methods and Supplementary Fig. 3). Fig. 3d shows that briefCO_2 resulted in an increase in H-Ruby fluorescence (i.e., a pH decrease) in pial arterioles after a delay of 2.0

bioRxiv preprint doi: https://doi.org/10.1101/2024.04.10.588509; this version posted April 14, 2024. The copyright holder for this preprint (which was not certified by peer review) is the author/funder, who has granted bioRxiv a license to display the preprint in perpetuity. It is made available under aCC-BY-NC-ND 4.0 International license.

± 0.7 s (n = 5 vessels, 4 mice). Note that as opposed to the CO_2 delivery at the mouse nostril which plateaued within 2 s (Fig. 1b), the pH response did not saturate (Fig. 3d, lower left). The shape of the signal can be taken as a temporal marker of the inflow of acidified blood transporting CO_2 and reaching the arterioles. It thus explains the early signals triggered by briefCO_2: the hyperventilation, the blood velocity decrease and NVU cell decreases of GCaMP6/8 fluorescence. Based on the properties of H-Ruby, we estimated that vascular pH decreased by about 0.15 pH on average (see Methods), a very significant change but brief enough to not threaten the animal's vital prognosis. Overall, the results show that briefCO_2 strongly acidifies cells of the entire arteriolar NVU with a dynamic fast enough to investigate the role of pH/CO_2 in NVC.

CO_2 does not interact with NVC measured at the arteriolar and capillary level

NVC involves several signaling pathways that may differ according to the site of neural excitation, i.e. at the level of arterioles or capillaries[32]. The onset of NVC occurs within ~1-2 s in rodents, with a time to peak between ~1-2 s for short stimulations and is modulated by anesthesia[24,33]. There is a consensus that in addition to the activation of astrocytes and pericytes, synaptic activation increases local potassium concentration, which generates a backpropagating signal along the vascular arbor, dilating large capillaries (also named the transitional segment[34]), and penetrating and pial arterioles[18,35]. In the somatosensory cortex, long CO_2 stimulation (10%, 10 min) was shown to result in markedly decreased NVC, an effect attributed to the saturation of CO_2-dependent processes (i.e. to an "occlusion" of the response) triggered by neuronal activation and resulting in NVC[17]. The timing of briefCO_2 makes it possible to test the hypothesis that exogenous CO_2 alters NVC as CO_2 diffusion and acidification of the periarteriolar column precedes arteriole dilation by several seconds. NVC occurring within 0.5-1 s of neuronal activation (Fig. 3a inset) following whisker stimulation (5 Hz, 5 s) was triggered either simultaneously with CO_2 inhalation (before the arteriole acidification, i.e., control conditions) or 2 s after CO_2 inhalation (during NVU acidification) (Fig. 4a,b). Fig. 4c shows that neuronal responses (perivascular bulk calcium; Thy1-GCaMP6s mice) were not affected during CO_2 diffusion and acidification of the periarteriolar column. Note that the drop of GCaMP6 fluorescence following neuronal activation resulted from CO_2-induced acidosis and not from a delayed inhibition. In addition, the superposition of arteriole dilations in both conditions show that the first phase of dilation (the first 5-6 s leading to the dilation peak) was similarly not affected by CO_2 (Fig. 4d). To analyze the extent to which NVC and CO_2 vascular responses were additive or not, we compared the calculated summation of these responses measured separately (Fig. 4e) with the experimental responses to both stimuli (i.e. experimental summation), with whisker stimulation occurring either simultaneously with briefCO_2 (Fig. 4f) or with a 2 s delay (Fig. 4g). Fig. 4f-h shows that the calculated summation of separate responses and the experimental summation with the two stimulation paradigms are similar when considering the first 5-6 s of NVC (up to the response peak). This means that there is perfect additivity and no occlusion of the two responses during this period. Thus, the early period of CO_2 diffusion and acidification of the NVU does not influence the initiation of NVC, although it may influence the second phase of NVC (see Supplementary Figure 4 and Discussion).

We then tested whether NVC is altered at the capillary and the arteriolar levels during a long CO_2 stimulation, as in Hosford et al.[17] by evaluating RBC velocity responses in the capillary bed (vessels located ≥ 5th branching order) and blood flow responses in pial arteries during 14 minutes of CO_2 stimulation (10%, Fig. 4i). In addition to increased respiration rate and decrease of pH (~0.1 unit, see Supplementary Fig. 5), resting RBC velocity and blood flow slowly increased during the first minute and stabilized after 4-5 minutes (+ 37% ± 19 and + 62% ± 25, respectively) (Fig. 4j,o; see also Supplementary Movie 2). Even under this condition of higher blood flow due to long hypercapnia, whisker stimulation generated similar RBC velocity and neuronal responses at the level of the capillary bed (Fig. 4k-n), as well as similar dilation and blood flow responses at the level of the arteries (Fig. 4p-s). Our approach suggests that, at the level of single arterioles and capillaries, CVR_{CO2} does not interact with NVC.

bioRxiv preprint doi: https://doi.org/10.1101/2024.04.10.588509; this version posted April 14, 2024. The copyright holder for this preprint (which was not certified by peer review) is the author/funder, who has granted bioRxiv a license to display the preprint in perpetuity. It is made available under aCC-BY-NC-ND 4.0 International license.

CO_2 does not affect NVC measured at the regional level

In humans, NVC and CVR_{CO2} are mostly evaluated with BOLD fMRI, i.e., with mesoscopic resolution. We thus used fUS to investigate the extent to which CO_2 interacts with CBV responses to whisker stimulation in the whole barrel cortex. We first evaluated the contribution of the arteriolar versus capillary compartments by comparing responses of slow (0.5-1.5 mm/s) and fast (> 3.5 mm/s) flowing CBV (i.e., the CBV fraction flowing with a low or high axial velocity[36]) to either whisker stimulation or CO_2 inhalation. Using co-registered TPLSM and fUS imaging in a single voxel, we have previously shown that slow flowing CBV is an excellent reporter of capillary responses during NVC[37]. Fig. 5a,b shows that in contrast to whisker stimulation, briefCO_2 led to an increase in fast, but not slow, CBV in the barrel cortex. This is in contrast to measurements at the capillary level with two-photon microscopy (Fig. 5c), which revealed small and delayed RBC velocity responses. This suggests that slow vascular responses to CO_2 are too small to be detected with fUS. Note that the dynamic of RBC velocity responses mimicked blood flow (arteriole level, Fig. 2b) and fast CBV (Fig. 5d) responses. Finally, we tested the effect of 14 minutes of CO_2 (10%) stimulation; Fig. 5d-f shows that functional hyperemia persisted during the "occlusion experiment", i.e. on top of increased resting blood flow due to CO_2, and that neither fast nor slow CBV responses were affected by CO_2. This demonstrates that NVC and CVR_{CO2} do not interrogate the same cerebrovascular reflexes.

Discussion

Here, we address the role of CO_2 produced by neuronal activation in generating NVC in layer 2/3 of the barrel cortex. All of our experiments were performed in chronic rather than acute preparations, as they preserve better brain metabolism[7]. We introduce briefCO_2, a specific short and strong CO_2 stimulation that triggers sharp vascular and cellular responses in brain vessels and cells, and allows repetitive applications. We used an analysis based on response onsets, which previously revealed the compartmentalization of NVC[18,24]. Our results reveal that in response to briefCO_2, vascular and cellular responses occur with two main response times, an early response within ~2 s of CO_2 inhalation, and a delayed response within ~6 s of CO_2 inhalation.

Early responses included the RBC velocity drop in brain arterioles, the increase in respiration rate, the decrease in pH measured in arterioles and a decrease in GCaMP fluorescence in all cells of the NVU. fUS measurements in the internal carotid show that the arteriole velocity drop may result from an early decrease of fast CBV in the carotid, which occurs concomitantly with an early decrease of mean arteriole pressure. We did not further investigate the mechanisms underlying the early CBV drop as it did not involve the brain *per se*. The onset of hyperventilation was rapid. Considering the speed of blood flow and the vascular distances for blood, loaded with CO_2, to reach either brain stem respiratory centers or the barrel cortex, we can assume that with the temporal resolution of our measurements, the pH drop occurs with "similar" onsets in the two brain regions. Similarly, we cannot distinguish which of peripheral or central chemoreceptors are first involved in the response[38–41]. The important point, rather, is that the vascular pH indicates that blood transporting CO_2 reaches brain arterioles within 2 s, a delay compatible with the time required for blood, acidified in the lung, to reach the cortex[28]. Acidification of NVU cells was fast. Our measurements are indirect as they are based on decreased fluorescence of GCaMP6/8 in NVU cells. Because this decrease occurs in all cells and it is known that pH changes, as large as those caused by briefCO_2 (0.15 of pH unit), can lead to a decrease in fluorescence of GFP or Ca^{2+} protein sensors such as GCaMP or R-GECO[29,42], thus we believe that they report intracellular acidosis rather than true calcium changes, although some calcium changes may be masked by acidosis, in particular in SMCs. In these cells, the drop of calcium due to NVC starts less than 400 ms before arteriole dilation [18]. This brief delay is thus 7 times smaller than the delay (~3 s) occurring between the fluorescence drop and dilation due to briefCO_2. It indicates that if some calcium decrease truly occurs upon CO_2, it is masked and involves a different signaling pathway than that triggered

bioRxiv preprint doi: https://doi.org/10.1101/2024.04.10.588509; this version posted April 14, 2024. The copyright holder for this preprint (which was not certified by peer review) is the author/funder, who has granted bioRxiv a license to display the preprint in perpetuity. It is made available under aCC-BY-NC-ND 4.0 International license.

during NVC. Note that it is also possible that CO_2 affects the frequency of some calcium hot spots in astrocytes, endothelial cells or SMCs, as our approach was not developed for their observation. A previous *in vivo* study reported that 10% of CO_2 stimulation (30 s) generated large and slow increases of OGB1 fluorescence in cortical astrocytes[43]. We recorded only a decrease in reporter signal, a difference that can be partially ascribed to the fact that our CO_2 stimulation was brief and our mice were sedated and not deeply anesthetized with α–chloralose. Overall, the pH-sensitivity of fluorescent sensors can lead to misinterpretations but can also be used to monitor intracellular acidosis.

Delayed responses to briefCO_2 include significant increases in arteriole diameter and flow, but only minor increases in blood velocity in capillaries. This contrasts with the strong velocity response in capillaries to whisker stimulation. These findings are supported by fUS measurements, which show a strong global increase of CBV flowing at high velocity, but no detectable response for CBV flowing at low velocity in response to briefCO_2. During NVC, both slow and fast CBVs increase. The small increase of blood velocity in the capillary bed during briefCO_2 is intriguing. It may result from blood redistribution throughout the entire capillary bed, as opposed to the more confined increase occurring during NVC. Although our CBV measurements do not support the hypothesis, it could also involve a blood redirection in-depth, as CO_2 dilation was suggested to be more important in arterioles from deep layers than from layer 2/3[44]. It is thus important to consider that NVC and CVR_{CO2} explore different vascular beds, in addition to the fact that CVR_{CO2} also shows a regional specificity[45].

In rodents, NVC onset occurs within ~1-2 s with an initial response peaking at about ~1-2 s (for brief stimulations) and, depending on the stimulation strength, a delayed response that involves astrocytes [46,47]. In our work, we have principally investigated the role of CO_2 on the initial component of NVC, the goal being to determine whether CO_2 is a necessary mediator to trigger NVC. We find that NVC remains robust under the two conditions of CO_2 stimulation. (1) briefCO_2, a strong stimulation during which CO_2 diffusion through the blood brain barrier must be massive, rapid, and limited in time. Our measurement of the intracellular acidosis onset in a given cell type indicates the maximum time necessary for CO_2 to reach that cell. In other words, acidosis may vary in amplitude and dynamics according to the expression of transporters and channels participating in cell-specific pH regulation. The fact that the decrease in fluorescence observed seemed faster in astrocytes than in endothelial cells or SMCs, despite astrocytes being further from the arteriole wall, indicates that CO_2 had already passed the first two cell types and that astrocytes have specific machinery to rapidly buffer brain acidification[13,48]. Therefore, if CO_2 *per se* has an effect on these three cells types, which participate in triggering local NVC, the initial phase of NVC should have been affected. In the case of perivascular neurons, it may be more complex; although probable, there is no proof that some CO_2 already diffused within the periarteriole dendritic neuropil when they responded to whisker stimulation, given that acidosis was not yet detected. It is thus not surprising that the neuronal response remained constant. However, NVC clearly occurred during acidosis and CO_2 diffusion: NVC and CO_2 responses showed full additivity during the first 6 seconds of NVC. A delayed second phase (or hump) appears during "paired" stimulation experiments. The shape of the hump depends on the timing of the summation. However, the difference between experimental and calculated summation of both NVC and CO_2 responses suggests a possible modulation of this late phase by acidosis (Supplementary Figure 4c). Although the investigation of this possible modulation is beyond the scope of our study, many mechanisms could be hypothesized, such as the degree of actin/myosin filament overlap in SMCs at the onset of second dilation or an effect of CO_2 on the mechanisms underlying the undershoot that terminates the NVC response. (2) Prolonged CO_2 (10%) stimulation, which should discard the objection that potential CO_2-dependent processes were not altered or "saturated" by briefCO_2. Surprisingly, NVC was not affected even after 14 minutes, although resting CBV and RBC velocity increased in both the arteriolar and capillary compartments. This implies that dilated arterioles could further dilate under neural activation. This is in line with some previous studies based on lower concentrations of inhaled CO_2[49,50], but does not support the recent work of Hosford et al. using prolonged 10% CO_2[17]. A major difference between the two studies is that our whisker stimulation is a mild sensory stimulation while paw electrical stimulation likely stimulates pain fibers in addition to sensory fibers, and it is known that

bioRxiv preprint doi: https://doi.org/10.1101/2024.04.10.588509; this version posted April 14, 2024. The copyright holder for this preprint (which was not certified by peer review) is the author/funder, who has granted bioRxiv a license to display the preprint in perpetuity. It is made available under aCC-BY-NC-ND 4.0 International license.

hypercapnia elevates pain threshold and depresses nociception[51]. Another difference may reside in our chronic sedated mouse preparation versus the α-chloralose anesthetized ventilated rat model. In our preparation, animals were free to hyperventilate to compensate acidosis and intravascular pH dropped by 0.1 pH unit while parenchymal pH decreased by 0.2 unit in Hosford's experimental conditions during prolonged CO_2 stimulation. This could also account for some of the differences. Still, even if our acidosis is lighter, it is important and NVC is perfectly preserved in the different vascular compartments. CVR to CO_2 and the signaling pathways involved have been thoroughly investigated in rodents and humans [19–21,52–54]. Here, we restricted our study to the analysis of timing. briefCO_2 stresses that CO_2 rapidly affects both peripheral and central circulation. The timing of events observed revealed that relaxation of SMCs lagged by ~3-4s after the drop in GCaMP6 fluorescence (i.e., cell acidosis), in contrast to what occurs during NVC, where relaxation occurs ~400 ms after a true decrease in calcium[18]. The signaling mechanisms linking acidosis to relaxation are thus distinct, slow and beyond the scope of our study. Overall, our data suggest that hypercapnia and thus probably endogenous CO_2 produced by neurons do not affect NVC, which principally depends on transmitter release and a rise in extracellular potassium[1,2,35]. In addition, it shows that NVC and CVR to CO_2 should be considered as two stimuli exploring distinct cerebrovascular reflexes with different dynamics, NVC being extremely rapid and CVR to CO_2 requiring a couple of seconds to occur and probing different vascular compartments.

bioRxiv preprint doi: https://doi.org/10.1101/2024.04.10.588509; this version posted April 14, 2024. The copyright holder for this preprint (which was not certified by peer review) is the author/funder, who has granted bioRxiv a license to display the preprint in perpetuity. It is made available under aCC-BY-NC-ND 4.0 International license.

References

1. Attwell, D. *et al.* Glial and neuronal control of brain blood flow. *Nature* 468, 232–43 (2010).

2. Iadecola, C. The Neurovascular Unit Coming of Age: A Journey through Neurovascular Coupling in Health and Disease. *Neuron* 96, 17–42 (2017).

3. Thompson, J. K., Peterson, M. R. & Freeman, R. D. Single-Neuron Activity and Tissue Oxygenation in the Cerebral Cortex. *Science* 299, 1070–1072 (2003).

4. Lecoq, J. *et al.* Odor-evoked oxygen consumption by action potential and synaptic transmission in the olfactory bulb. *J. Neurosci. : Off. J. Soc. Neurosci.* 29, 1424–33 (2009).

5. Masamoto, K. *et al.* Biphasic changes in tissue partial pressure of oxygen closely related to localized neural activity in guinea pig auditory cortex. *J. Cereb. blood flow Metab. : Off. J. Int. Soc. Cereb. Blood Flow Metab.* 23, 1075–84 (2003).

6. Lecoq, J. *et al.* Simultaneous two-photon imaging of oxygen and blood flow in deep cerebral vessels. *Nat Med* 17, 893–898 (2011).

7. Aydin, A.-K., Verdier, C., Chaigneau, E. & Charpak, S. The oxygen initial dip in the brain of anesthetized and awake mice. *Proc National Acad Sci* 119, e2200205119 (2022).

8. Wei, H. S. *et al.* Erythrocytes Are Oxygen-Sensing Regulators of the Cerebral Microcirculation. *Neuron* 91, 851–862 (2016).

9. Chhabria, K. *et al.* The effect of hyperglycemia on neurovascular coupling and cerebrovascular patterning in zebrafish. *J. Cereb. Blood Flow Metab.* 40, 298–313 (2018).

10. Powers, W. J., Hirsch, I. B. & Cryer, P. E. Effect of stepped hypoglycemia on regional cerebral blood flow response to physiological brain activation. *Am J Physiol-heart C* 270, H554–H559 (1996).

11. Nippert, A. R., Chiang, P.-P. & Newman, E. A. Whisker-evoked neurovascular coupling is preserved during hypoglycemia in mouse cortical arterioles and capillaries. *J. Cereb. Blood Flow Metab.* 271678X231201241 (2023) doi:10.1177/0271678x231201241.

12. Venton, B. J., Michael, D. J. & Wightman, R. M. Correlation of local changes in extracellular oxygen and pH that accompany dopaminergic terminal activity in the rat caudate-putamen: Correlation of oxygen and pH changes. *J. Neurochem.* 84, 373–381 (2003).

13. Theparambil, S. M. *et al.* Astrocytes regulate brain extracellular pH via a neuronal activity-dependent bicarbonate shuttle. *Nat Commun* 11, 5073 (2020).

14. Stawarski, M. *et al.* Neuronal Glutamatergic Synaptic Clefts Alkalinize Rather Than Acidify during Neurotransmission. *J. Neurosci.* 40, 1611–1624 (2020).

15. Kontos, H. A., Raper, A. J. & Patterson, J. L. Analysis of vasoactivity of local pH, PCO2 and bicarbonate on pial vessels. *Stroke* 8, 358–360 (1977).

16. Michenkova, M. *et al.* Carbon dioxide transport across membranes. *Interface focus* 11, 20200090 (2021).

17. Hosford, P. S. *et al.* CO2 signaling mediates neurovascular coupling in the cerebral cortex. *Nat Commun* 13, 2125 (2022).

18. Rungta, R. L., Chaigneau, E., Osmanski, B.-F. & Charpak, S. Vascular Compartmentalization of Functional Hyperemia from the Synapse to the Pia. *Neuron* 99, 362-375.e4 (2018).

19. Sleight, E., Stringer, M. S., Marshall, I., Wardlaw, J. M. & Thrippleton, M. J. Cerebrovascular Reactivity Measurement Using Magnetic Resonance Imaging: A Systematic Review. *Front Physiol* 12, 643468 (2021).

20. Liu, P., Vis, J. B. D. & Lu, H. Cerebrovascular reactivity (CVR) MRI with CO2 challenge: A technical review. *Neuroimage* 187, 104–115 (2019).

bioRxiv preprint doi: https://doi.org/10.1101/2024.04.10.588509; this version posted April 14, 2024. The copyright holder for this preprint (which was not certified by peer review) is the author/funder, who has granted bioRxiv a license to display the preprint in perpetuity. It is made available under aCC-BY-NC-ND 4.0 International license.

21. Caldwell, H. G., Carr, J. M. J. R., Minhas, J. S., Swenson, E. R. & Ainslie, P. N. Acid–base balance and cerebrovascular regulation. *J Physiology* 599, 5337–5359 (2021).

22. Mateo, C., Knutsen, P. M., Tsai, P. S., Shih, A. Y. & Kleinfeld, D. Entrainment of Arteriole Vasomotor Fluctuations by Neural Activity Is a Basis of Blood-Oxygenation-Level-Dependent "Resting-State" Connectivity. *Neuron* 96, 936-948.e3 (2017).

23. Winder, A. T., Echagarruga, C., Zhang, Q. & Drew, P. J. Weak correlations between hemodynamic signals and ongoing neural activity during the resting state. *Nat Neurosci* 20, 1761–1769 (2017).

24. Rungta, R. L. *et al.* Diversity of neurovascular coupling dynamics along vascular arbors in layer II/III somatosensory cortex. *Commun Biology* 4, 855 (2021).

25. Macé, E. *et al.* Functional ultrasound imaging of the brain. *Nat Methods* 8, 662–664 (2011).

26. Brunner, C. *et al.* A Platform for Brain-wide Volumetric Functional Ultrasound Imaging and Analysis of Circuit Dynamics in Awake Mice. *Neuron* 108, 861-875.e7 (2020).

27. Deffieux, T., Demené, C. & Tanter, M. Functional Ultrasound Imaging: A New Imaging Modality for Neuroscience. *Neuroscience* 474, 110–121 (2021).

28. Zhang, Q. *et al.* Cerebral oxygenation during locomotion is modulated by respiration. *Nat Commun* 10, 5515 (2019).

29. Helassa, N., Podor, B., Fine, A. & Török, K. Design and mechanistic insight into ultrafast calcium indicators for monitoring intracellular calcium dynamics. *Sci Rep-uk* 6, 38276 (2016).

30. Cho, J.-H. *et al.* The GCaMP-R Family of Genetically Encoded Ratiometric Calcium Indicators. *Acs Chem Biol* 12, 1066–1074 (2017).

31. Despras, G. *et al.* H-Rubies, a new family of red emitting fluorescent pH sensors for living cells. *Chem. Sci.* 6, 5928–5937 (2015).

32. Mishra, A. *et al.* Astrocytes mediate neurovascular signaling to capillary pericytes but not to arterioles. *Nat Neurosci* 19, 1619–1627 (2016).

33. Franceschini, M. A. *et al.* The effect of different anesthetics on neurovascular coupling. *NeuroImage* 51, 1367–1377 (2010).

34. Ratelade, J. *et al.* Reducing Hypermuscularization of the Transitional Segment Between Arterioles and Capillaries Protects Against Spontaneous Intracerebral Hemorrhage. *Circulation* 141, 2078–2094 (2020).

35. Longden, T. A. *et al.* Capillary K+-sensing initiates retrograde hyperpolarization to increase local cerebral blood flow. *Nat Neurosci* 20, 717–726 (2017).

36. Boido, D. *et al.* Mesoscopic and microscopic imaging of sensory responses in the same animal. *Nat Commun* 10, 1110 (2019).

37. Aydin, A.-K. *et al.* Transfer functions linking neural calcium to single voxel functional ultrasound signal. *Nat Commun* 11, 2954 (2020).

38. Gourine, A. V. *et al.* Astrocytes Control Breathing Through pH-Dependent Release of ATP. *Science* 329, 571–575 (2010).

39. Wang, S. *et al.* TASK-2 Channels Contribute to pH Sensitivity of Retrotrapezoid Nucleus Chemoreceptor Neurons. *J Neurosci* 33, 16033–16044 (2013).

40. Kumar, N. N. *et al.* Regulation of breathing by CO_2 requires the proton-activated receptor GPR4 in retrotrapezoid nucleus neurons. *Science* 348, 1255–1260 (2015).

41. SheikhBahaei, S. *et al.* Contributions of carotid bodies, retrotrapezoid nucleus neurons and preBötzinger complex astrocytes to the CO2-sensitive drive for breathing. *J. Physiol.* (2023) doi:10.1113/jp283534.

bioRxiv preprint doi: https://doi.org/10.1101/2024.04.10.588509; this version posted April 14, 2024. The copyright holder for this preprint (which was not certified by peer review) is the author/funder, who has granted bioRxiv a license to display the preprint in perpetuity. It is made available under aCC-BY-NC-ND 4.0 International license.

42. Molina, R. S. *et al.* Understanding the Fluorescence Change in Red Genetically Encoded Calcium Ion Indicators. *Biophys. J.* 116, 1873–1886 (2019).

43. Howarth, C. *et al.* A Critical Role for Astrocytes in Hypercapnic Vasodilation in Brain. *J Neurosci* 37, 2403–2414 (2017).

44. Hotta, H. *et al.* Layer-Specific Dilation of Penetrating Arteries Induced by Stimulation of the Nucleus Basalis of Meynert in the Mouse Frontal Cortex. *J Cereb Blood Flow Metabolism* 33, 1440–1447 (2013).

45. Thrippleton, M. J. *et al.* Cerebrovascular reactivity measurement in cerebral small vessel disease: Rationale and reproducibility of a protocol for MRI acquisition and image processing. *Int J Stroke* 13, 195–206 (2017).

46. Institoris, A. *et al.* Astrocytes amplify neurovascular coupling to sustained activation of neocortex in awake mice. *Nat. Commun.* 13, 7872 (2022).

47. Schulz, K. *et al.* Simultaneous BOLD fMRI and fiber-optic calcium recording in rat neocortex. *Nat Methods* 9, 597–602 (2012).

48. Gourine, A. V. & Dale, N. Brain H+ /CO2 sensing and control by glial cells. *Glia* 70, 1520–1535 (2021).

49. Nishino, A. *et al.* Vasodilation Mechanism of Cerebral Microvessels Induced by Neural Activation under High Baseline Cerebral Blood Flow Level Results from Hypercapnia in Awake Mice. *Microcirculation* 22, 744–752 (2015).

50. Kennerley, A. J. *et al.* Early and Late Stimulus-Evoked Cortical Hemodynamic Responses Provide Insight into the Neurogenic Nature of Neurovascular Coupling. *J. Cereb. Blood Flow Metab.* 32, 468–480 (2011).

51. Gamble, G. D. & Milne, R. J. Hypercapnia depresses nociception: endogenous opioids implicated. *Brain Res.* 514, 198–205 (1990).

52. Iadecola, C. & Zhang, F. Permissive and obligatory roles of NO in cerebrovascular responses to hypercapnia and acetylcholine. *Am J Physiology-regulatory Integr Comp Physiology* 271, R990–R1001 (1996).

53. Dabertrand, F., Nelson, M. T. & Brayden, J. E. Acidosis Dilates Brain Parenchymal Arterioles by Conversion of Calcium Waves to Sparks to Activate BK Channels. *Circ Res* 110, 285–294 (2012).

54. Hartmann, D. A. *et al.* Brain capillary pericytes exert a substantial but slow influence on blood flow. *Nat Neurosci* 24, 633–645 (2021).

55. Tournissac, M. *et al.* Cranial window for longitudinal and multimodal imaging of the whole mouse cortex. *Proc Spie* 9, 031921 (2022).

56. Diaz, J. R., Kim, K. J., Brands, M. W. & Filosa, J. A. Augmented astrocyte microdomain Ca2+ dynamics and parenchymal arteriole tone in angiotensin II-infused hypertensive mice. *Glia* 67, 551–565 (2019).

57. Rungta, R. L., Osmanski, B.-F., Boido, D., Tanter, M. & Charpak, S. Light controls cerebral blood flow in naive animals. *Nat Commun* 8, 14191 (2017).

58. Renaudin, N. *et al.* Functional ultrasound localization microscopy reveals brain-wide neurovascular activity on a microscopic scale. *Nat Methods* 19, 1004–1012 (2022).

59. Ganesh, K., Soumen, R., Ravichandran, Y. & Janarthanan. Dynamic approach to predict pH profiles of biologically relevant buffers. *Biochem. Biophys. Rep.* 9, 121–127 (2017).

60. Chaigneau, E. & Charpak, S. Measurement of Blood Velocity With Laser Scanning Microscopy: Modeling and Comparison of Line-Scan Image-Processing Algorithms. *Front Physiol* 13, 848002 (2022).

bioRxiv preprint doi: https://doi.org/10.1101/2024.04.10.588509; this version posted April 14, 2024. The copyright holder for this preprint (which was not certified by peer review) is the author/funder, who has granted bioRxiv a license to display the preprint in perpetuity. It is made available under aCC-BY-NC-ND 4.0 International license.

Methods

Animals

All animal care and experimentations were performed in accordance with the INSERM Animal Care and Use Committee guidelines and approved by the ethical committee (Charles Darwin, comité national de réflexion éthique sur l'expérimentation animale n°5) (protocol number #27135 2020091012114621) and animal care and use committee of Augusta University. Mice were fed ad libitum and housed in a 12-hour light-dark cycle. Adult mice, both males and females, from 3 to 10 months of age were included. The following mouse lines were used and bred in our animal facility: C57/BL6J, NG2-CreER^{TM},Ai95(RCL-GCaMP6f), Thy1-GCaMP6s (GP4.3), Cdh5-GCaMP8 (#033342, Jackson Laboratory), VeCadh-CreERT2,Ai95(RCL-GCaMP6f), Cx30-CreERT2 were crossed with Ai95-GCaMP6f mice to generate Cx30-CreERT2;Ai95-GCaMP6f mice, Aldh1l1-Cre/ERT2 (#031008, Jackson Laboratory) were crossed with Ai95-GCaMP6f mice to generate Aldh1l1-CreERT2;Ai95-GCaMP6f mice. GCaMP6 expression by CreERT2 recombination was induced by the administration of 1 mg of Z-4-hydroxy-tamoxifen (4-OHT, Tocris #3412) (0.2 mL, 20 mg/mL, i.p.) per mouse per day for three consecutive days.

Surgery and sedation

Chronic cranial windows were implanted one week after the head bar surgery as described[55]. We used a 100 µm-thick glass coverslip over the barrel cortex for TPLSM (~3mm^2) and a 100 µm-thick polymethylpentene (PMP) coverslip over the entire neocortex for fUS experiments. A recovery period of 7-10 days minimum was respected before imaging experiments. During imaging sessions, mice were sedated with continuous perfusion of dexmedetomidine as follows: induction of anesthesia was done with 3% isoflurane and then decreased by 0.5% every 5 min down to 0% within 30 min, and dexmedetomidine was administered with a bolus (0.025 mg/kg s.c.) at the beginning of the session and a s.c. perfusion (0.1 mg/kg/h) during the entire session. Texas Red (70 kDa dextran, D1830, LifeTechnologies) or the pH-sensitive dye (see below) were administered intravenously (i.v.) with a retro-orbital injection prior to the decrease in isoflurane (under 3-2.5% isoflurane). Recordings started 20 minutes after the isoflurane cutoff. Body temperature was controlled with a rectal probe and maintained at 36.5°C with a feedback-controlled heating pad. The animal was monitored throughout the imaging session using an infrared webcam (DCC3240N, Thorlabs).

Hypercapnic and whisker stimulations

Hypercapnic and whisker stimulations were delivered with a homemade setup controlled with a custom Labview software (National Instruments). Mice received air supplemented with oxygen to reach a final concentration of 28% O_2 continuously through a nose cone. A valve, controlled electronically, was used to switch rapidly the mixture from air only to air and CO_2. The concentration of CO_2 at the mouse nostril was measured before each experiment to ensure that a 20% or a 10% plateau was reached within 2 s (SprintIR-R CO_2 sensor, Gas Sensing Solutions). Hypercapnic stimulations were repetitively applied with a minimum of 5 min interstimulus interval. Unilateral whisker deflections of the entire pad were achieved with a moving bar (5 Hz, 5 s). Both stimulations were triggered with the acquisition setup.

Respiration measurement

Breathing was monitored during each imaging acquisition using a thermocouple placed in front of one nostril[37]. The respiratory rate (Hz) was extracted from the downward deflections due to inhalations.

Arterial pressure and heart rate measurements

Blood pressure was assessed in a subgroup of C57/BL6 male mice implanted with a telemetry transmitter device (PA-C10, Data Sciences) under isoflurane[56]. The catheter of the device was inserted in the left carotid artery. Mice were housed individually and a recovery period of at least one week was respected before the experiments. Hypercapnic stimulations were performed as described above under dexmedetomidine sedation and breathing rate was monitored. Blood pressure signals were

bioRxiv preprint doi: https://doi.org/10.1101/2024.04.10.588509; this version posted April 14, 2024. The copyright holder for this preprint (which was not certified by peer review) is the author/funder, who has granted bioRxiv a license to display the preprint in perpetuity. It is made available under aCC-BY-NC-ND 4.0 International license.

sampled at 100 Hz. Systolic and diastolic arterial pressure were extracted with peaks and valleys detected using a custom Matlab script. The mean blood pressure was calculated as the mean value between each valley and consecutive peak. The heart rate was calculated by extracting the time between each peak (i.e. systolic events, corresponding to heart beats), and then converted to beats per minutes (bpm).

Two-photon laser scanning microscopy

Imaging was performed using a femtosecond laser (Mai Tai eHP; SpectraPhysics) with a dispersion compensation module (Deepsee; SpectraPhysics) emitting 70-fs pulses at 80 MHz. Laser power was attenuated by an acoustic optical modulator (AA Optoelectronic, MT110-B50-A1.5-IR-Hk). Scanning was performed with Galvanometric scanner (GS) mirrors (8315KM60B; Cambridge Technology). AF488 and H-Ruby were excited at 880 nm and GCaMP6, GCaMP8, and Texas Red were excited at 920 nm. Emitted light was collected with either a LUMFLN60XW (Olympus, 1.1 NA) or a LUMPLFLN40XW (Olympus, 0.8NA) water immersion objective. Collected photons were sorted according to their wavelength using a dichroic mirror centered at 570 nm and the following filters: FF01-525/25 nm filter (Semrock) for AF488; FF01-609/62 for H-Ruby and FF01-620/20 for Texas Red. Photons were collected with 2 GaAsP (Hamamatsu) photomultipliers tubes. Customized LabView software was used to control the system.

fUS imaging and data analysis

Cerebral blood volume (CBV) measurements were acquired using an ultrasound scanner (Iconeus One, Iconeus) as described previously[55,57]. Briefly, we used a linear ultrasound probe (128 elements, 15 MHz central frequency, Vermon) with an ultrasound sequence consisting of transmitting 11 different tilted plane waves (from −10° to 10° in 2° increments) with a 5500-Hz pulse repetition frequency (500 Hz frame rate of reconstructed images). Post-processing analysis was done in Matlab (version R2018a, MathWorks) with a custom-made software: the first 40 singular value decomposition (SVD) were removed and the power Doppler (PD) signal was further filtered with a Butterworth filter (fifth order). Data are shown as ΔPD/PD, with a baseline of 9 s (from 1 to 10 s). CBV flowing at low (10-30 Hz, 0.5-1.5 mm/s) and high (> 60 Hz, > 3 mm/s) axial velocities were separated by filtering as previously described[36]. In a subset of experiments, ultrasound localization microscopy (ULM) was used to measure the velocity of gas microbubbles injected i.v. (100 µL bolus, retro-orbital injection, Sonovue, Braco) and recorded with a 3 minutes acquisition (8V, superlocalization mode)[58].

Functionalization of dextran with H-Ruby

H-Ruby dextran was obtained from the click reaction between H-Ruby-N_3 and a clickable dextran (70 kDa). The protocol for synthesis and characterizations can be found in Supplementary Informations. To a solution of H-Ruby-N_3 (2.5 mg, 4.1 µmol) and clickable dextran 70 kDa (30 mg, 0.3 µmol) in 400 µL degassed DMF was added copper sulfate pentahydrate (5 mg) and sodium ascorbate (5 mg) in water (100 µL). The reaction was stirred in the dark at 40°C for 30 min. DMF was evaporated and the crude residue was dissolved in aq. 0.1 M EDTA (1 mL) to remove traces of cupper salt, purified over Sephadex® G-25 size exclusion column and lyophilized to obtain H-Ruby dextran conjugate as a pink solid (28 mg, molar ratio ~ 3 mol dye/mol dextran). A similar protocol was applied to obtain AF488 dextran conjugate, using AF488 azide (Lumiprobe GmbH, Hannover, Germany).

pKa determination of H-Ruby Dextran conjugate

Fluorescence spectra of H-Ruby Dextran conjugate (excitation: 530 nm, 0.9 µM of fluorophore) were recorded using a FluoroMax-4 spectrofluorometer (Horiba Jobin Yvon) and pH-controlled buffers (ranging from pH 4.5 to pH 10.5) using a mixture of boric acid, citric acid and phosphate buffers according to the literature[59]. Fluorescence intensity at 580 nm was plotted against the pH and a Sigmoidal DoseResp fit provided the pKa value of 7.57 ± 0.18.

pH measurements

bioRxiv preprint doi: https://doi.org/10.1101/2024.04.10.588509; this version posted April 14, 2024. The copyright holder for this preprint (which was not certified by peer review) is the author/funder, who has granted bioRxiv a license to display the preprint in perpetuity. It is made available under aCC-BY-NC-ND 4.0 International license.

H-Ruby dextran (70 kDa, 0.6 mg/kg) and AF488 dextran (70 kDa, 2 mg/kg) were co-administrated i.v. by retro-orbital injection. pH was calculated from the ratio of the average red and average green fluorescence signals in a region of interest (ROI) inside the vessel after subtraction of their respective backgrounds: $FR = (F_{Red} - F_{RedBackground}) / (F_{Green} - F_{GreenBackground})$.
pH calculation was performed as follows:
1) A look-up table was established by measuring R of H-Ruby-dextran and AF488 dextran in pH-controlled samples of fresh rat blood plasma. Data was fitted with a sigmoid function: $FR = \alpha_{system} (R_{Range} / (1 + \exp (\alpha_{pH}(pH-pKa))) + R_{Cte})$ using nonlinear least square optimization for R_{Cte}, α_{pH} and pKa in MatLab (see supplementary Fig. 6). α_{system} is a constant specific to our microscope that characterizes the relative sensitivity of the system to the same amount of photons detected on the red channel or on the green channel. The following coefficients were obtained: $\alpha_{pH} = 2.64 \pm 2.1$, $pKa = 7.47 \pm 0.31$ and $R_{Cte} = 0.32 \pm 0.19$, $R^2 = 0.994$, error corresponding to 95 % confidence bound. Note that R_{Cte} is not zero as a significant part of AF488 emission spectrum corresponds to the detection spectrum of our red channel.
2) As H-Ruby maximum fluorescence not only depends on pH but also on its chemical environment, depth in the brain, and optical properties of the tissue, R_{Range} needs to be set for each recording. Therefore, R_{Range} was calculated for each recording as:
$R_{Range} = (FR_{Baseline} / \alpha_{system} - R_{cte}) (1 + \exp (\alpha_{pH} (7.4 - pKa)))$
where $FR_{Baseline}$ is the average FR in the baseline period where pH is assumed to be 7.4 in blood.
3) The pH was calculated as: $pH = pKa + \ln (R_{Range} / (FR / \alpha_{system} - R_{Cte}) - 1) / \alpha_{pH}$

Image analysis
Diameter change in pial arterioles and RBC velocity in arterioles and capillaries were determined with line-scan acquisitions as described previously [18]. The LSPIV method was used to compute RBC velocity in arterioles and the angle algorithm for velocity in capillaries[60]. Diameter changes of penetrating arterioles were quantified by measuring their lumen area from 3 Hz movies with a custom Matlab script. GCaMPs fluorescence signals over chosen ROIs were computed as $\Delta F/F = (F - F_0) / (F_0)$, where F_0 represents the fluorescence of the baseline and F the fluorescence at time t. For the analysis of endothelial and smooth muscle cell GCaMP fluorescence, measurements required correction for dilation movements: ROIs (1/3 to 1/2 of the cells) were selected and each frame was realigned (cross-correlation) according to the ROI (See Supplementary Movie 1 for more details).

Statistics and onset analysis
We computed our data in z score because of fluctuations in the baseline due to vasomotion[24]. Z score was calculated for each trial as follows: $z\ score = (x - \mu_{baseline}) / \sigma_{baseline}$ with a 9 s long baseline, , with $\mu_{baseline}$ the mean of the baseline, and $\sigma_{baseline}$ the standard deviation (SD) of the baseline. Trials from the same vessel were averaged (with a 0.1 s interpolation) for analysis. As the mathematical functions underlying the responses to briefCO_2 are currently unknown, model functions were first determined for each parameter measured (diameter, respiratory rate, RBC velocity, GCaMP fluorescence) using the average (all vessels) responses. Onsets were determined by fitting data from individual vessels with the specific model function and choosing the time to reach 10% of the peak of the fit. All fits were determined using the non-linear least mean square method for custom-made functions in Matlab. Details concerning the model fitting function determination for each parameter are available in Supplementary Table 1. Onsets of paired data and area under the curve of responses before and during CO_2 were analyzed using a non-parametric two-sided Wilcoxon rank sum test (GraphPad Prism, version 6). Data are represented as mean ± standard deviation.

Data availability
The data generated in the present study are available from the corresponding authors upon reasonable request.

Code availability

bioRxiv preprint doi: https://doi.org/10.1101/2024.04.10.588509; this version posted April 14, 2024. The copyright holder for this preprint (which was not certified by peer review) is the author/funder, who has granted bioRxiv a license to display the preprint in perpetuity. It is made available under aCC-BY-NC-ND 4.0 International license.

The codes used for the analyses are available from the corresponding author upon reasonable request. Matlab scripts used for onset determination are available online in the following GitHub repository: https://github.com/charpak-lab/Onset_fits_TournissacEtAl

Acknowledgements

We thank Manon Omnes for the management of mice colonies and performing some of the surgeries and Davide Boido for training M.T. to surgery and fUS experiments. We thank Kun Xie for his assistance during the blood pressure experiments. Fig. 4a was created with BioRender.com.

Financial support was provided by the Institut national de la santé et de la recherche médicale (Inserm), the European Research Council (ERC-2013-AD6; 339513), the Fondation pour la Recherche Médicale (EQU201903007811), the Agence Nationale de la Recherche (NR-16-RHUS-0004 [RHU TRT_cSVD], CE37_2020_TF-fUS-CADASIL and CE14-0026-01_Brain-mapping-of-pH-and-CO2), the Fondation Leducq Transatlantic Networks of Excellence program (16CVD05, Understanding the role of the perivascular space in cerebral small vessel disease), the Fondation Alzheimer France (M21JRCN009) and the IHU FOReSIGHT [ANR-18-IAHU-0001] supported by French state funds managed by the Agence Nationale de la Recherche within the Investissements d'Avenir program. M.T. was supported by a fellowship from the Fondation pour la Recherche Médicale (SPF201909009103).

Author contributions

M.T. and S.C. designed the study, interpreted the data and wrote the manuscript. M.T. performed and analyzed all experiments. A.J. participated to the conception of the project and the interpretation of the data. E.C. developed the onset measurement with fitting and the theoretical approach and software for pH measurements. A.-K.A. developed some scripts for fUS and two-photon analysis. Y.G. maintained the performances of our custom-built microscope and participated to set rapid and controlled CO_2 application system. S.F. and M.C. synthetized the pH sensors. P.O. and J.F. prepared the animals and helped with blood pressure and heart rate measurements. All authors edited the manuscript.

bioRxiv preprint doi: https://doi.org/10.1101/2024.04.10.588509; this version posted April 14, 2024. The copyright holder for this preprint (which was not certified by peer review) is the author/funder, who has granted bioRxiv a license to display the preprint in perpetuity. It is made available under aCC-BY-NC-ND 4.0 International license.

Figure Legends

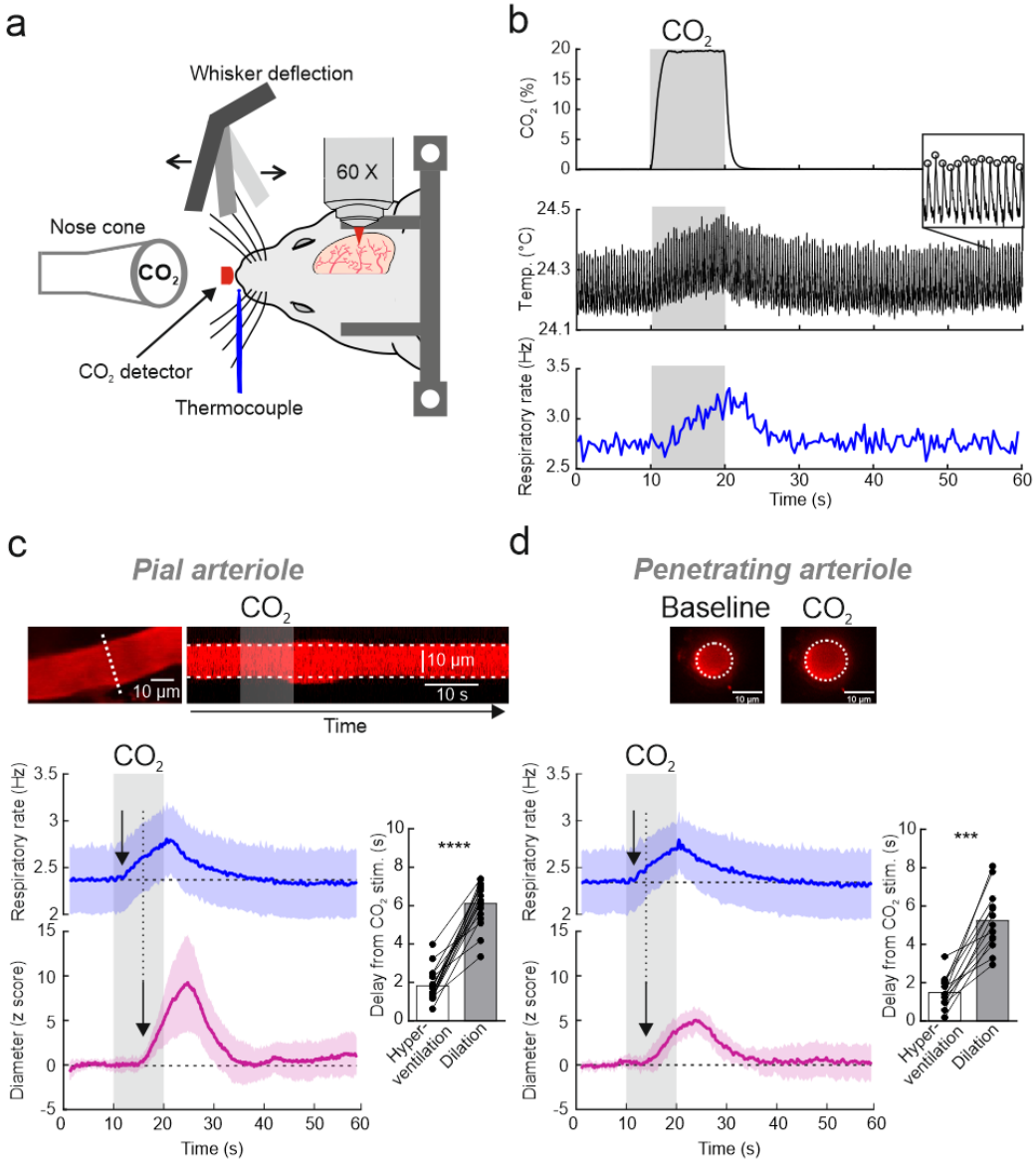

Fig.1 briefCO_2 stimulation generates early and delayed responses.

a, Head-fixed sedated mice, implanted with a chronic cranial window over the barrel cortex, were exposed to a brief and strong hypercapnic stimulation (briefCO_2: 20%, 10 s) or to whole pad whisker stimulation (5 Hz, 5 s). Respiration was monitored with a thermocouple placed in front of the nostril and blood flow imaged with two-photon imaging. **b,** Top, CO_2 concentration measured at the nostril, reached a plateau within 2 s. Middle and inset, detection of temperature peaks enabled the respiratory rate to be computed (bottom, single trial), which increased after a delay of about 2 s. **c,** Top left, a pial arteriole labelled with Texas Red injected IV. The diameter was measured with line-scan acquisitions drawn perpendicular to the vessel (white dotted line). Top right, Representative example of a pial arteriole dilation upon briefCO_2. Bottom left, Average responses to briefCO_2. Diameter changes are expressed in z score to minimize the contribution of spontaneous 0.1 Hz fluctuations. Dilation lagged the hyperventilation by ~4 s (see the arrows, paired data, n = 16 arterioles, 12 mice, 2-5 stimulations per vessel). Bottom right, quantification of the onsets (Wilcoxon rank sum test, ****$p < 0.0001$). **d,** Top, the diameter of penetrating arterioles was calculated from lumen area. Bottom left and right – as for pial arterioles, hyperventilation precedes dilation by ~4 s (paired data, n = 13 arterioles, 11 mice, 2-5 stimulations per vessel, Wilcoxon rank sum test, ***$p < 0.001$). The arrows indicate the onset time to reach 10% of the fit of the curves. Data are represented as mean ± SD.

bioRxiv preprint doi: https://doi.org/10.1101/2024.04.10.588509; this version posted April 14, 2024. The copyright holder for this preprint (which was not certified by peer review) is the author/funder, who has granted bioRxiv a license to display the preprint in perpetuity. It is made available under aCC-BY-NC-ND 4.0 International license.

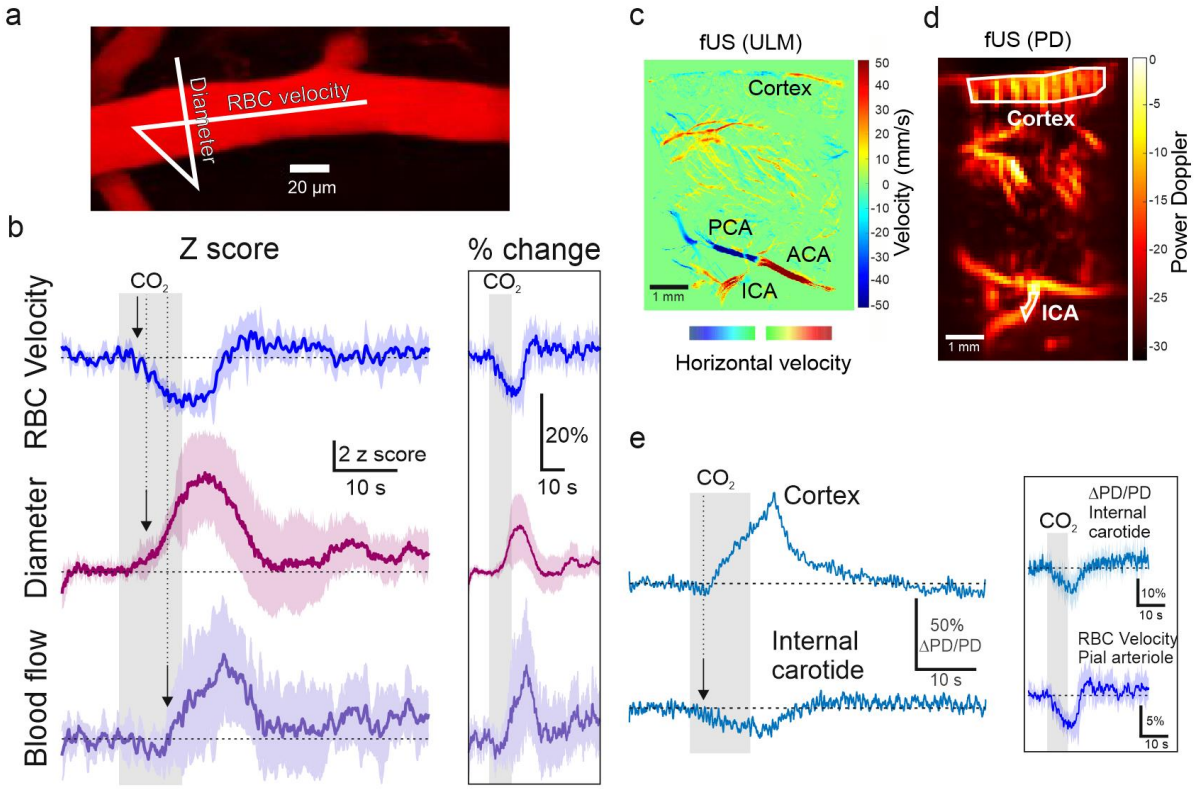

Fig.2 Uncoupling of arteriole diameter, blood velocity and blood flow during briefCO_2

a, Top, red blood cell (RBC) velocity and diameter were measured simultaneously with a broken line-scan drawn along and across the pial arteriole (white line). **b,** Upon briefCO_2, velocity decreases before the delayed arteriole dilation. Calculated blood flow (velocity * π.radius^2) shows a transient decrease followed by an increase due to dilation. Right inset shows data presented in percent change from baseline (n = 7 vessels, 6 mice). **c,** A sagittal section of a mouse brain was recorded with ultrasound localization microscopy (ULM) upon microbubbles injection (i.v.). This approach allowed to position CBV measurements in the internal carotid artery (ICA). Note that it also reported resting blood velocity, the color map representing the horizontal component of the RBC speed. **d,** Power Doppler image of the same sagittal section acquired with standard functional ultrasound imaging (fUS). A high-pass filter selecting the CBV flowing with an axial velocity > 8 mm/s was applied. **e,** Left, briefCO_2 generated a delayed increase in CBV in the cortex preceded by a small early drop, concomitant with an early CBV decrease in the ICA (average of 5 stimulations). Inset, comparison of the dynamics of CBV responses in the ICA (top, n = 6 experiments, 3-5 stimulations, 5 mice) and RBC velocity responses in pial arterioles (bottom, same trace as in panel b). The arrows indicate the onset time to reach 10% of the fit of the curves. Data are represented as mean ± SD.

bioRxiv preprint doi: https://doi.org/10.1101/2024.04.10.588509; this version posted April 14, 2024. The copyright holder for this preprint (which was not certified by peer review) is the author/funder, who has granted bioRxiv a license to display the preprint in perpetuity. It is made available under aCC-BY-NC-ND 4.0 International license.

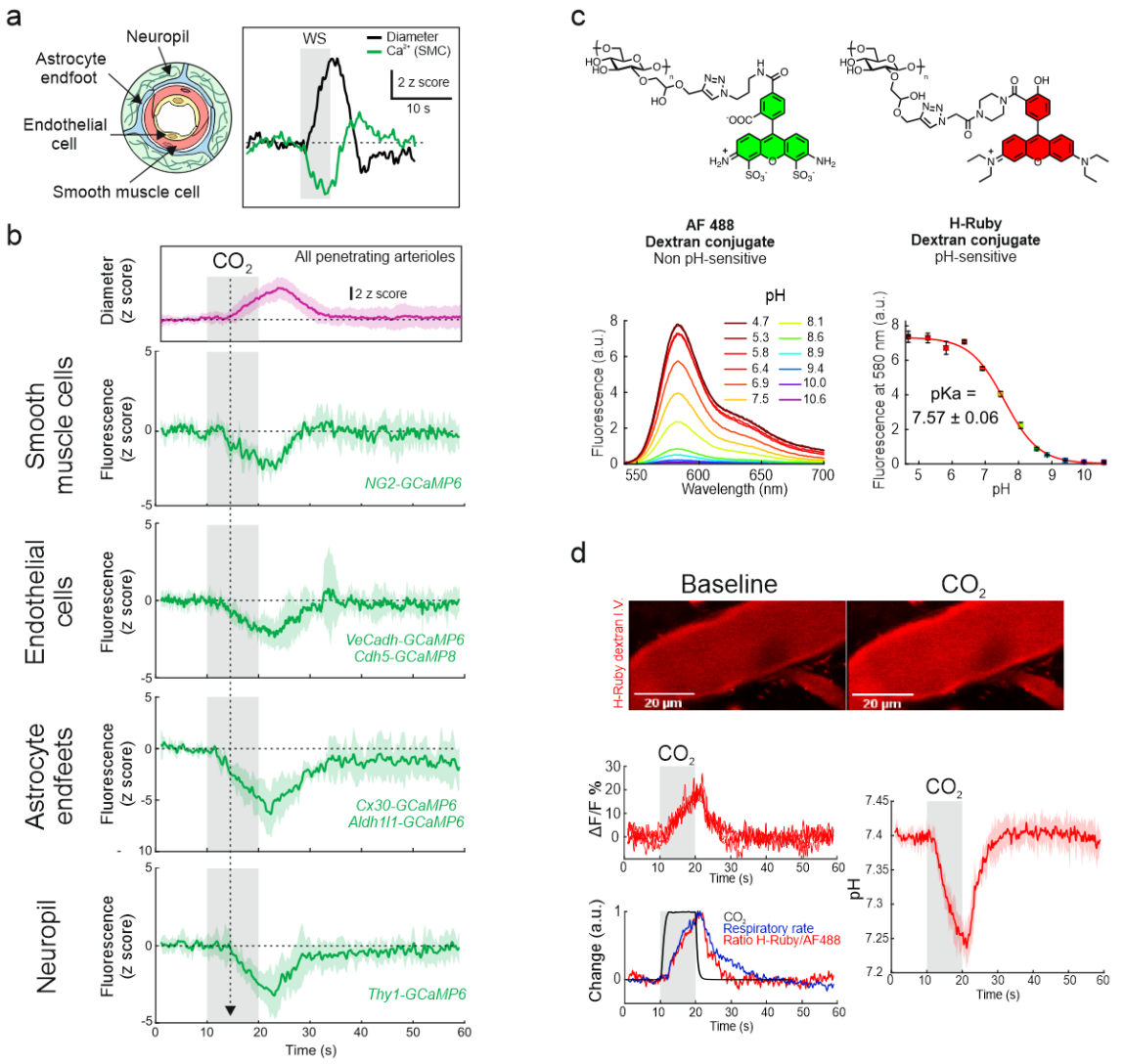

Fig.3 briefCO_2 acidifies the whole neurovascular unit of penetrating arterioles.

a, Left - Schematic representation of the different cells composing the neurovascular unit. Right – the inset illustrates the observation that during neurovascular coupling (whisker stimulation, WS), GCaMP6 fluorescence from smooth muscle cells (SMCs) decreased over a few hundred milliseconds (green trace) before dilation (black trace) (n = 4 vessels, 3 mice). **b,** Upon briefCO_2 stimulation, dilation of the penetrating arteriole was preceded by a decrease in GCaMP6 or GCaMP8 fluorescence in all cells of the neurovascular unit (note that fluorescence of each cell type was recorded individually in one of the six transgenic lines expressing either GCaMP6 or GCaMP8), suggesting that it may result from modulation of GCaMP fluorescence due to pH (n = 5-8 vessels, 4-6 mice). **c,** Top, H-Ruby (pH-sensitive) and AF488 (pH insensitive) fluorescent molecules functionalized to Dextran 70 kDa. Bottom left, fluorescence emission spectra of H-Ruby as a function of pH. Bottom right, H-Ruby fluorescence intensity curve as a function of pH. **d,** Top, H-Ruby fluorescence at rest (left) and during briefCO_2 (right). Bottom (top left), 5 consecutive responses to briefCO_2 showing a reproducible increase in fluorescence in plasma. Bottom left, superposition of normalized traces of respiratory rates, H-Ruby/AF488 fluorescence ratio and inhaled CO_2 concentration. Right, briefCO_2 caused a reversible pH decrease (0.15 pH units) with an onset of about 2 s (n = 5 vessels, 4 mice). The dotted arrow indicates the onset time to reach 10% of the fit of the dilation curve. Data are represented as mean ± SD.

bioRxiv preprint doi: https://doi.org/10.1101/2024.04.10.588509; this version posted April 14, 2024. The copyright holder for this preprint (which was not certified by peer review) is the author/funder, who has granted bioRxiv a license to display the preprint in perpetuity. It is made available under aCC-BY-NC-ND 4.0 International license.

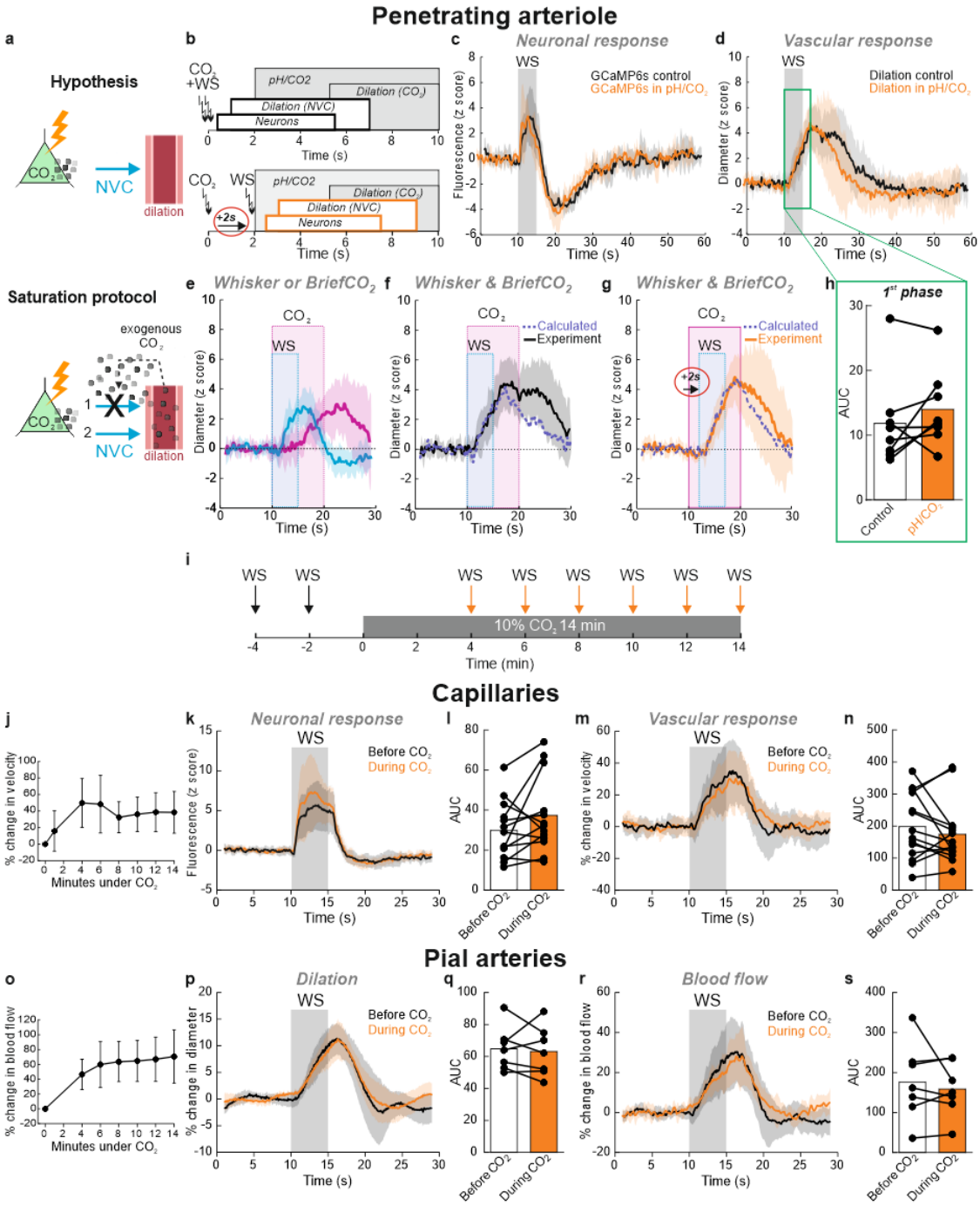

Fig.4 CO_2 does not interact with neurovascular coupling measured at the single vessel level.

a, Schematic of the hypothesis: Top, CO_2 produced by neurons initiates NVC. Bottom, exogenous CO_2 (briefCO_2 or continuous CO_2 stimulation) diffuses from vessels to the parenchyma and either 1) saturates CO_2-dependent mechanisms, blocking NVC or 2) does not affect NVC. **b,** "Paired stimulation" paradigm: top, briefCO_2 and whisker stimulation (WS) are triggered at the same time; neuronal activation and dilation due to NVC occurred before CO_2 reached the arteriole NVU. Bottom, whiskers were stimulated 2 s after the onset of briefCO_2. As a result, NVC occurred during CO_2 diffusion and acidification of the arteriole wall and its surrounding neuronal parenchyma. **c**, Neuronal responses (increase in Ca^{2+}) remained constant during briefCO_2. Note that the secondary decrease in GCaMP6 fluorescence was due to acidosis (n = 5 vessels, 4 mice). **d,** BriefCO_2 does not affect the initiation of dilation due to NVC (n = 9 vessels, 4 Thy1Gc6 mice in which Ca^{2+} was simultaneously measured and 2 C57BL/6 mice). **e,** Vascular responses to whisker (blue trace) or briefCO_2 (pink trace) measured separately. **f,** Calculated summation of the vascular responses in e (dotted purple line) and

bioRxiv preprint doi: https://doi.org/10.1101/2024.04.10.588509; this version posted April 14, 2024. The copyright holder for this preprint (which was not certified by peer review) is the author/funder, who has granted bioRxiv a license to display the preprint in perpetuity. It is made available under aCC-BY-NC-ND 4.0 International license.

experimental data (black solid line) of the responses to whisker (5 Hz, 5 s) and briefCO2 (20% CO2, 10 s) stimulations applied at the same time. **g,** Calculated summation (dotted purple line) and experimental data (orange solid line) when whisker stimulation is delayed by 2 s from the onset of briefCO_2. **h,** AUC for area under the curve during the initiation of NVC (green box) calculated between 10-17 s for control and 12-19 s for pH/CO2 condition considering the 2 s delay. Paired data, Wilcoxon sum rank test, ns, p = 0.25, n = 8 vessels, 5 mice. The first 7 s of NVC response are similar in both conditions (f,g) showing a perfect additivity of the two responses. Data are represented as mean ± SD. **i,** "Continuous" CO_2 stimulation paradigm: WS was applied before or during prolonged hypercapnia (10% CO_2 for 14 min). **j,** Upon continuous CO_2, resting capillary RBC velocity progressively increased, reaching a plateau at 4 minutes. **k and l,** Neuronal responses were similar before and during CO_2 exposure (n = 13 vessels, 6 mice). **m and n,** Functional hyperemia was not affected by long CO_2 exposure (n = 14 vessels, 7 mice). **o,** Resting blood flow increased in pial arteries upon continuous CO_2. **p-s,** Dilation and blood flow increase in response to whisker stimulation was similar before and during prolonged hypercapnia (n = 7 vessels, 3 mice). **l,n,q,s,** Area under the curve (AUC) between 10 and 20 s (paired data, Wilcoxon sum rank test, ns). Data are represented as mean ± SD.

bioRxiv preprint doi: https://doi.org/10.1101/2024.04.10.588509; this version posted April 14, 2024. The copyright holder for this preprint (which was not certified by peer review) is the author/funder, who has granted bioRxiv a license to display the preprint in perpetuity. It is made available under aCC-BY-NC-ND 4.0 International license.

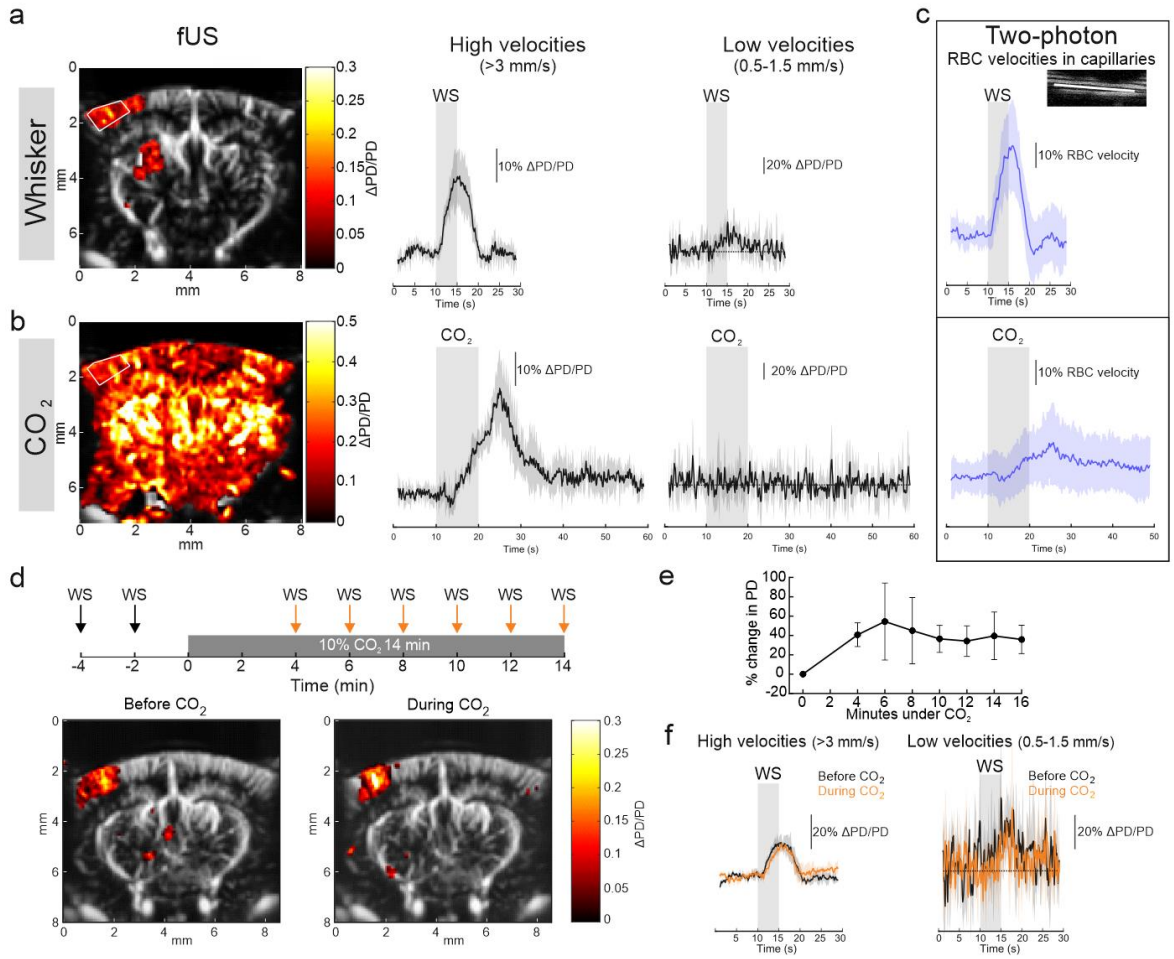

Fig.5 CO_2 does not interact with neurovascular coupling measured at the regional level.

a, Left, activated voxels (ΔPD/PD) in response to whisker stimulation (WS) (5 s, 5 Hz) superimposed on the Power Doppler image of a coronal section of the mouse brain (average of 4 stimulations). Right, ΔPD/PD responses to WS in the barrel cortex (ROI framed by the white lines). Axial velocities were filtered to separate CBV flowing at high (> 3 mm/s) and low (> 0.5-1.5 mm/s) speed, corresponding to large and small (capillaries) vessels respectively (n = 6 experiments, 5 mice). Note the small responses at low velocity. **b,** Left, activation map in response to briefCO_2 showing a widespread activation throughout the brain (average of 4 stimulations, same brain section as above for WS). Right, ΔPD/PD responses for high and low velocities (same ROI as for WS) showing no detectable responses to briefCO_2 in small vessels (n = 5 experiments, 5 mice). **c,** Responses to briefCO_2 were however detectable in capillaries with two-photon microscopy (n = 44 vessels, 25 mice), although much smaller than during WS (n = 23 vessels, 15 mice). **d,** Top, schematic of the occlusion paradigm. Bottom - Activated voxels (ΔPD/PD) superimposed on the Power Doppler map showing similar response to WS applied before (left) or during (right) prolonged CO_2 stimulation (10%, 14 min). **e,** Resting CBV increased upon continuous CO_2 application as represented by the percent change in resting Power Doppler. **f,** Increased CBV to WS for high (left) and low (right) axial velocity is similar in control or during prolonged hypercapnia (n = 4 experiments, 3 mice). Data are represented as mean ± SD.